1-1-2014

The structured core domain of αB-crystallin can prevent amyloid fibrillation and associated toxicity

Georg K. A Hochberg
University of Oxford

Heath Ecroyd
University of Wollongong, heathe@uow.edu.au

Cong Liu
Howard Hughes Medical Institute

Dezerae Cox
University of Wollongong, dcc356@uowmail.edu.au

Duilio Cascio
University of California

See next page for additional authors

The structured core domain of αB-crystallin can prevent amyloid fibrillation and associated toxicity

Abstract

Mammalian small heat-shock proteins (sHSPs) are molecular chaperones that form polydisperse and dynamic complexes with target proteins, serving as a first line of defense in preventing their aggregation into either amorphous deposits or amyloid fibrils. Their apparently broad target specificity makes sHSPs attractive for investigating ways to tackle disorders of protein aggregation. The two most abundant sHSPs in human tissue are αB-crystallin (ABC) and HSP27; here we present high-resolution structures of their core domains (cABC, cHSP27), each in complex with a segment of their respective C-terminal regions. We find that both truncated proteins dimerize, and although this interface is labile in the case of cABC, in cHSP27 the dimer can be cross-linked by an intermonomer disulfide linkage. Using cHSP27 as a template, we have designed an equivalently locked cABC to enable us to investigate the functional role played by oligomerization, disordered N and C termini, subunit exchange, and variable dimer interfaces in ABC. We have assayed the ability of the different forms of ABC to prevent protein aggregation in vitro. Remarkably, we find that cABC has chaperone activity comparable to that of the full-length protein, even when monomer dissociation is restricted through disulfide linkage. Furthermore, cABC is a potent inhibitor of amyloid fibril formation and, by slowing the rate of its aggregation, effectively reduces the toxicity of amyloid-β peptide to cells. Overall we present a small chaperone unit together with its atomic coordinates that potentially enables the rational design of more effective chaperones and amyloid inhibitors.

Keywords

CMMB

Disciplines

Medicine and Health Sciences | Social and Behavioral Sciences

Publication Details

Hochberg, G. K. A., Ecroyd, H., Liu, C., Cox, D., Cascio, D., Sawaya, M., Collier, M., Stroud, J., Carver, J. A., Baldwin, A. J., Robinson, C. V., Eisenberg, D., Benesch, J. & Laganowsky, A. (2014). The structured core domain of αB-crystallin can prevent amyloid fibrillation and associated toxicity. Proceedings of the National Academy of Sciences of USA, 111 (16), E1562-E1570.

Authors

Georg K. A Hochberg, Heath Ecroyd, Cong Liu, Dezerae Cox, Duilio Cascio, Michael Sawaya, Miranda Collier, James Stroud, John A. Carver, Andrew Baldwin, Carol Robinson, David Eisenberg, Justin Benesch, and Arthur Laganowsky

A structured core domain of αB-crystallin can prevent amyloid fibrillation and associated toxicity

Georg K.A. Hochberg[1,*], Heath Ecroyd[2,*], Cong Liu[3], Dezerae Cox[2], Duilio Cascio[3], Michael R. Sawaya[3], Miranda P. Collier[1], James Stroud[3], John A. Carver[4], Andrew J. Baldwin[1], Carol V. Robinson[1], David Eisenberg[3], Justin L.P. Benesch[1,†], and Arthur Laganowsky[1,3,†]

[1]Department of Chemistry, Physical and Theoretical Chemistry Laboratory, University of Oxford, South Parks Road, Oxford, OX1 3QZ, U.K. [2]Illawarra Health and Medical Research Institute and School of Biological Sciences, University of Wollongong, Wollongong, NSW 2522, Australia [3]Howard Hughes Medical Institute, UCLA-DOE Institute for Genomics and Proteomics, Department of Chemistry and Biochemistry, University of California, Los Angeles, Los Angeles, CA 90095-1570, U.S.A. [4]Research School of Chemistry, The Australian National University, Canberra, ACT 0200, Australia. * These authors contributed equally to this work. † Correspondence to: JLPB (justin.benesch@chem.ox.ac.uk; +44 1865 285420) and AL (art.laganowsky@chem.ox.ac.uk; +44 1865 275965)

Submitted to Proceedings of the National Academy of Sciences of the United States of America

Mammalian small heat-shock proteins (sHSPs) are molecular chaperones that form polydisperse and dynamic complexes with target proteins, serving as a first line of defence in preventing their aggregation into either amorphous deposits or amyloid fibrils. Their apparently broad target specificity makes sHSPs attractive for investigating how to tackle disorders of protein aggregation. The two most abundant sHSPs in human tissue are αB-crystallin (ABC) and HSP27; here we present high-resolution structures of their core domains (cABC, cHSP27), each in complex with a segment of their respective C-terminal regions. We find that both truncated proteins dimerise, and while this interface is labile in the case of cABC, in cHSP27 the dimer can be cross-linked by an inter-monomer disulphide linkage. Using cHSP27 as a template we have designed an equivalently locked cABC to enable us to investigate the functional role played by oligomerisation, disordered N- and C- termini, subunit exchange and variable dimer interfaces in ABC. We have assayed the ability of the different forms of ABC to prevent protein aggregation in vitro, and remarkably find that cABC has chaperone activity comparable to the full-length protein, even when monomer dissociation is restricted through disulphide linkage. Furthermore, cABC is a potent inhibitor of amyloid fibril formation, and, by slowing the rate of its aggregation, effectively reduces the toxicity of amyloid-β peptide to cells. Overall we present a small chaperone unit together with its atomic coordinates that potentially enable the rational design of more effective chaperones and amyloid inhibitors.

αB-crystallin | small heat-shock protein | molecular chaperone | amyloid | X-ray crystallography

Introduction

The proteome is inherently metastable (1, 2), and therefore the cell is required to actively maintain protein homeostasis (or "proteostasis") through the balancing of a multitude of biochemical pathways (3). The breakdown of this steady state can lead to a variety of diseases, many of which are characterised by the aggregation and deposition of misfolded proteins (4). Molecular chaperones, proteins that act to prevent improper polypeptide associations, are crucial components of the cellular proteostasis machinery (5, 6). They include the small heat-shock proteins (sHSPs), which are found in organisms across all branches of the tree of life and play an important role in preventing protein misfolding and aggregation (7, 8). In general the sHSPs are capable of intercepting destabilized targets (9), and either: holding them in a refolding competent state; preventing them from aggregating into unrecoverable deposits; or directing them towards degradation (10). αB-crystallin (ABC) is an abundant mammalian sHSP, the expression of which is constitutive in most human tissues and upregulated in a variety of pathological disorders (11). The chaperone activity of ABC has been established for over two decades (12), and it is associated with amyloid fibril deposits *in vivo* that are characteristic of protein misfolding diseases including Alzheimer's and Parkinson's diseases (13-15).

Proteins enter the amyloid cascade from their native state and form insoluble fibrils via various intermediates, including oligomeric forms (16, 17). Both amyloid fibrils and oligomers are harmful to cells, however the latter appear to be more toxic (18). ABC has been shown to mitigate amyloid toxicity to cells in culture (19), to interact directly with amyloid oligomers *in vitro* (20), and to prevent the fibrillation of a variety of targets (21-25). Additionally ABC has been shown to bind to mature amyloid-β peptide ($A\beta_{1\text{-}42}$) (22, 24), α-synuclein (23, 25), and apolipoprotein C-II (apoC-II) fibrils (26), apparently coating them and preventing their elongation (21). An understanding of how ABC carries out these activities has been hindered by the structural and dynamical complexities of this chaperone. ABC, as is typical for most metazoan sHSPs, consists of a dimeric building block that assembles via terminal interactions into a polydisperse ensemble (8). In ABC, these oligomers range from approximately 10 to 50 subunits and readily interconvert via the exchange of monomers (27), in a process that facilitates the formation of heterooligomers between different sHSPs (28). While several new models have recently been developed for ABC oligomers, a consensus as to their quaternary structure remains to be reached (8, 29).

The sequence of ABC can be divided into an immunoglobulin-like "α-crystallin domain" (ACD) that mediates

Significance

We find that the core domain of the human molecular chaperone αB-crystallin can function effectively in preventing protein aggregation and amyloid toxicity. The core domain represents only half the total sequence of the protein, yet it is one of the most potent known inhibitors of the aggregation of amyloid-β, a process implicated in Alzheimer's disease. We have determined high-resolution structures of this core domain, and investigated its biophysical properties in solution. Our findings reveal that the excised domain efficiently prevents amyloid aggregation and thereby reduces the toxicity of the resulting aggregates to cells. The structures we present of these domains should represent useful scaffolds for the design of novel amyloid inhibitors.

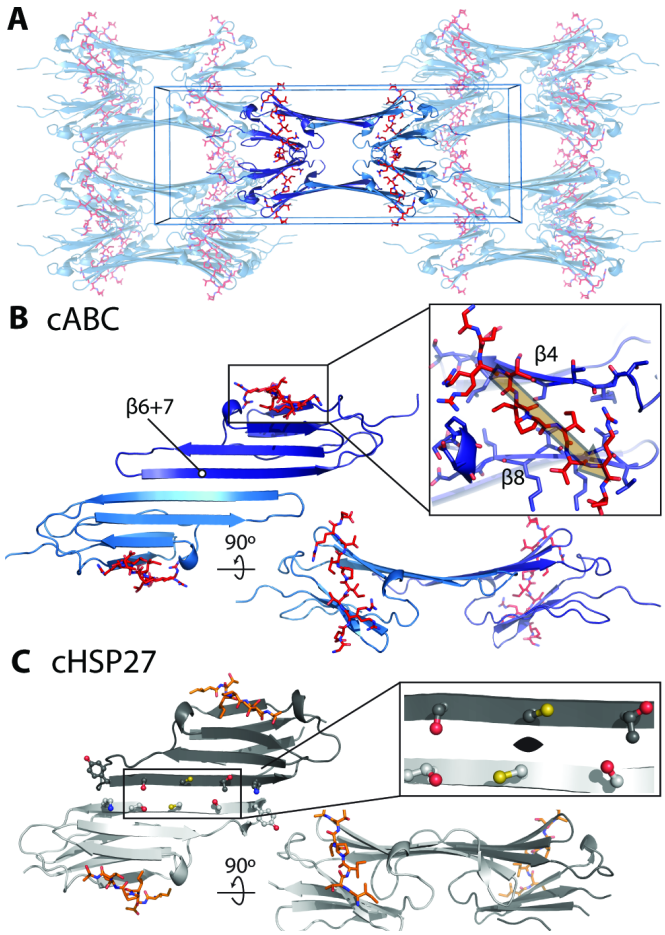

Fig. 1. Crystal structures of cABC and cHSP27. **(A)** cABC crystallizes as a dimer of dimers, with one C-terminal peptide of sequence ERTIPITRE (red) bound to each monomer. **(B)** Two immunoglobulin-like cABC monomers assemble into a dimer through pairwise and anti-parallel interactions between extended β6+7 strands. In this structure the dimer is found in the AP_{III} register. The palindromic C-terminal peptide binds to a hydrophobic groove between β4 and β8 strands, in an anti-parallel direction to the β8 strand (inset, direction N to C illustrated by yellow arrow). **(C)** The crystal structure of cHSP27 reveals a dimer similar to cABC, rich in β sheet structure and with C-terminal peptides bound. cHSP27 however is in the AP_{II} register, with C137 (thiol coloured in yellow) located about a two-fold axis at the dimer interface (inset). C137 is reduced in the structure due to the presence of reductant during crystallisation, but can readily be oxidised (Fig. 4).

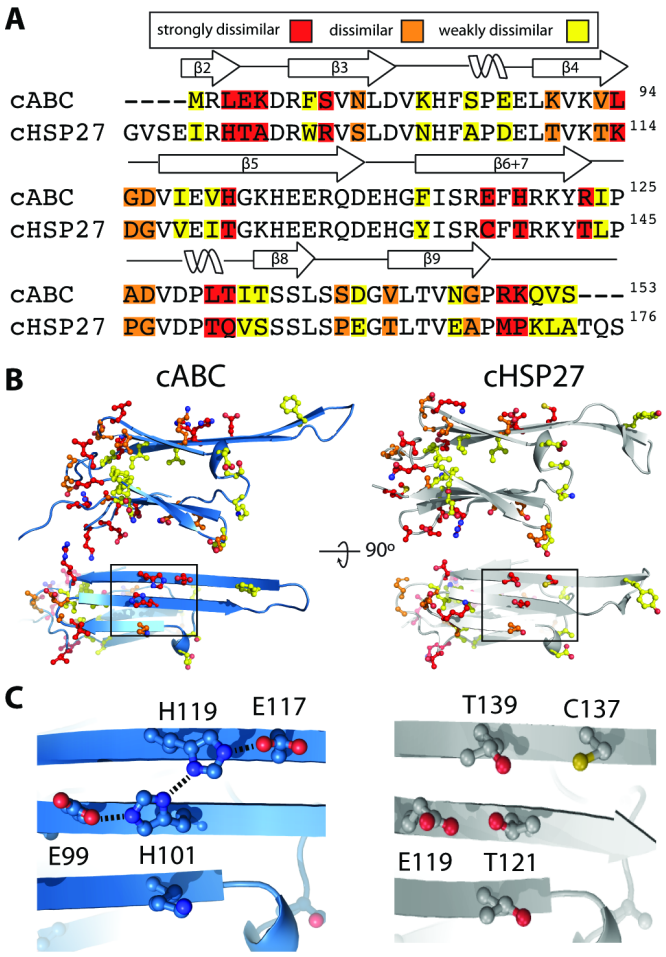

Fig. 2. Structural differences between cHSP27 and cABC. **(A)** Sequence alignment of the two domains coloured to highlight differences in amino-acid composition (strongly dissimilar, red; dissimilar, orange; weakly dissimilar, yellow, see methods). The two domains are clearly highly similar (54.7 % identity), though differences are distributed throughout the sequence. **(B)** Mapping the disparate residues on the cABC (left) and cHSP27 (right) structures (colouring as in **A**) reveals them to be spread over the entire structure. **(C)** An expansion of the boxed region in **B** reveals a charge network formed by residues E99, H101, E117, and H119 in cABC (left) that is absent in cHSP27 (right) where the equivalent residues are E119, T139, T121 and C137.

dimerization, and is flanked by N- and C-terminal regions that are poorly conserved and variable in length between sHSPs (7, 8). Various regions of the ABC sequence have been implicated as potential binding sites, but there is little consensus (30-34). Moreover, it even remains unclear whether the polydisperse oligomeric ensemble of ABC, the oligomeric dissociation that mediates subunit exchange, or remodelling of the dimer interface is responsible for chaperone function (8). Models have been proposed wherein sub-oligomeric forms, which are in equilibrium with the assembled state, are the active chaperoning unit. This idea is based on the observation that solution conditions that accelerate subunit exchange also lead to increased chaperone activity (35). Conversely, other studies have demonstrated that ABC can still function as a chaperone despite being cross-linked as an oligomer (36), and that mutations that slow its subunit exchange kinetics do not necessarily diminish its activity as a chaperone *in vitro* (37).

These apparent conflicts likely stem from the intrinsic heterogeneity of ABC and the difficulty in assessing the interplay between its structural and dynamical aspects (8, 29). Here we have gained insight into the chaperone activity of ABC, and the prevention of protein aggregation in general, by establishing a minimal, yet chaperone-active, unit of ABC that is suitable for structural studies. We drew inspiration from recent structures of the ACD that have revealed the ABC dimer interface to be composed of paired "β6+7" strands (38-41). Interestingly, their anti-parallel interaction has been crystallized in two different registers, termed AP_I and AP_{II} (41), with a third (AP_{III}) having been found for the related HSP20 (38). The three registrations have different amounts of buried surface area in the dimer interface, resulting from monomers being progressively shifted outward relative to one another in AP_{II} and AP_{III} relative to AP_I. We have engineered a construct comprising exclusively the core domain of ABC (cABC), which allowed us to test the relationship between oligomeric state, subunit exchange, registration state, and chaperone function of ABC.

Our experimental strategy combines X-ray crystallography with native mass spectrometry (MS) and nuclear magnetic resonance spectroscopy (NMR) to examine the structure of cABC. Using a novel approach to crystallise the protein we show that

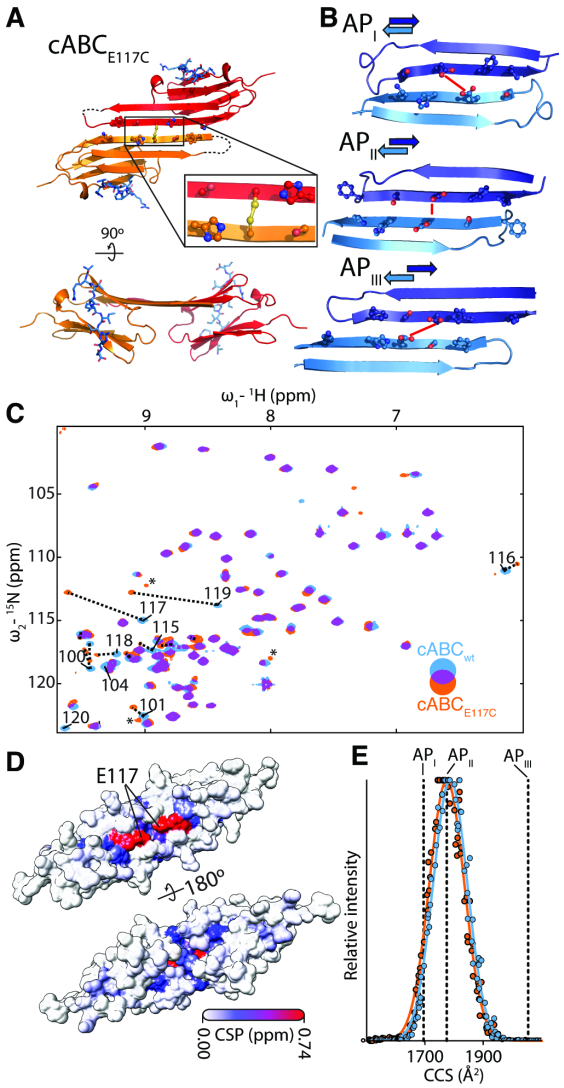

Fig. 3. NMR and IM reveal AP_{II} as the dominant registration state for cABC in solution. **(A)** Crystal structure of $cABC_{E117C}$ in which the introduced cysteine acts to lock the domain into a dimer in the AP_{II} register. The disulphide bond formed between two monomers is shown in the inset. The overall structure of this engineered ACD is closely similar to that of cABC. **(B)** The three registers of the ABC dimer observed by X-ray crystallography: AP_I (PDB ID: 3L1G), AP_{II} (2WJ7), and AP_{III} (present work, 4M5S). Red lines indicate the vector between α-carbons of residues E117 on the two monomers, which is located on a two-fold axis in AP_{II}. The distance between two modelled cysteines at position 117 is close enough for disulphide bond formation only in AP_{II} (9.13 Å between the two thiols in AP_I, 0.93 Å in AP_{II}, and 6.5 Å in AP_{III}). **(C)** ^{1}H-^{15}N-HSQC spectra of cABC (blue) $cABC_{E117C}$ (orange) acquired under identical and oxidizing solution conditions. Overlap of peaks is represented by purple. Peaks with significant shifts in the mutant are labelled on the plot. Dotted lines indicate peak movement in the mutant compared to cABC, and asterisks unassigned peaks. The spectra overlay very well, indicating that the fold of the two proteins is very similar. **(D)** A heat map of CSP projected onto the structure of cABC (largest CSP, red; lowest, white) reveals that the most significant changes in chemical shift are observed near C117. **(E)** IM measurements of the cABC (blue) and $cABC_{E117C}$ (orange) 7+ charge state (see Fig. 4E,F) under oxidizing conditions reveal very similar CCS distributions. Dashed lines indicate anticipated CCS values of AP_I, AP_{II}, and AP_{III}. As the CCS distribution of cABC matches that of $cABC_{E117C}$, which is fixed as an AP_{II} dimer, we can infer that cABC preferentially populates the AP_{II} register.

cABC can populate three different registers, and that the AP_{II} form is predominantly populated in solution. Through comparison with a new structure of the HSP27 core domain (which

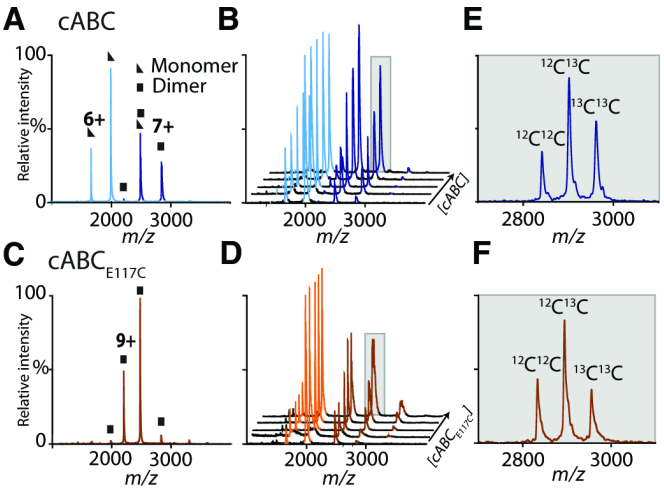

Fig. 4. Quaternarydynamics of cABC and $cABC_{E117C}$. **(A)** Nanoelectrospray MS of cABC reveals two charge state distributions corresponding to an equilibrium of monomers (triangles) and dimers (squares). **(B)** A titration series of cABC reveals an increase in the abundance of dimer (dark blue) relative to monomer (light blue) as the concentration is increased (2, 4, 8, 16 and 32 μM, front to back). Spectra are normalized such that the most intense peak in each spectrum is equal to 100%. The shaded area indicates the 7+ charge state of the dimer. **(C)** A mass spectrum of $cABC_{E117C}$, obtained under the same conditions as for cABC in **A**, reveals the exclusive presence of dimers due to disulphide bond formation. **(D)** In the presence of reductant $cABC_{E117C}$ reverts to a concentration-dependent equilibrium of monomers (orange) and dimers (brown) (concentrations as in **B**) **(E)** A mass spectrum of unlabelled cABC mixed with ^{13}C-labelled cABC, acquired as soon as possible, and focussing solely on the 7+ charge state (shaded in **C**). Both homo- and heterodimers are observed, indicating rapid subunit exchange. **(F)** An equivalent experiment to that in **E** carried out with $cABC_{E117C}$ under reducing conditions demonstrates fast subunit exchange as observed for cABC.

we also present here), we have engineered a cysteine mutant of cABC ($cABC_{E117C}$) that can be locked into a dimeric state in the AP_{II} registration. This protein is therefore unable to exchange monomers under oxidizing conditions. We show that both cABC and $cABC_{E117C}$ can strongly inhibit amorphous aggregation, amyloidogenesis and amyloid toxicity, all as effectively as the wild-type protein. Together our data demonstrate that the core domain of ABC is responsible for its potent molecular chaperone function, which is retained regardless of stoichiometry or registration state of the dimer.

Results

An alternative strategy to crystallise mammalian sHSPs

In a novel approach to crystallise mammalian ACDs, we designed a system composed of a core unit of ABC (residues 68-153, cABC), and a peptide mimicking its C-terminal region (residues 156-164, ERTIPITRE), to avoid the runaway domain swapping that resulted in a polymer-like crystal array in our previous study (41). Co-crystallisation of cABC and the peptide produced crystals that led to structure determination at 1.35 Å (Table S1). The structure of cABC reveals a crystal packing of tetrameric units, assembled essentially as a dimer of dimers (Fig. 1A). One peptide is bound to each cABC monomer in an orientation anti-parallel to the β8 strand (Fig. 1B), the inverse of that in our previous structure of ABC (41). This bi-directionality is enabled by the palindromic nature of the peptide (42), and is consistent with the binding observed in NMR experiments (43). The two monomers form a dimer interface in which they are slightly bent relative to each other (Fig. 1A), reminiscent of a structure of ABC obtained by means of solid-state NMR (40) (Fig. S1). The angle between monomers is however larger in our structure, reflecting a flatter interface, and we also observe no

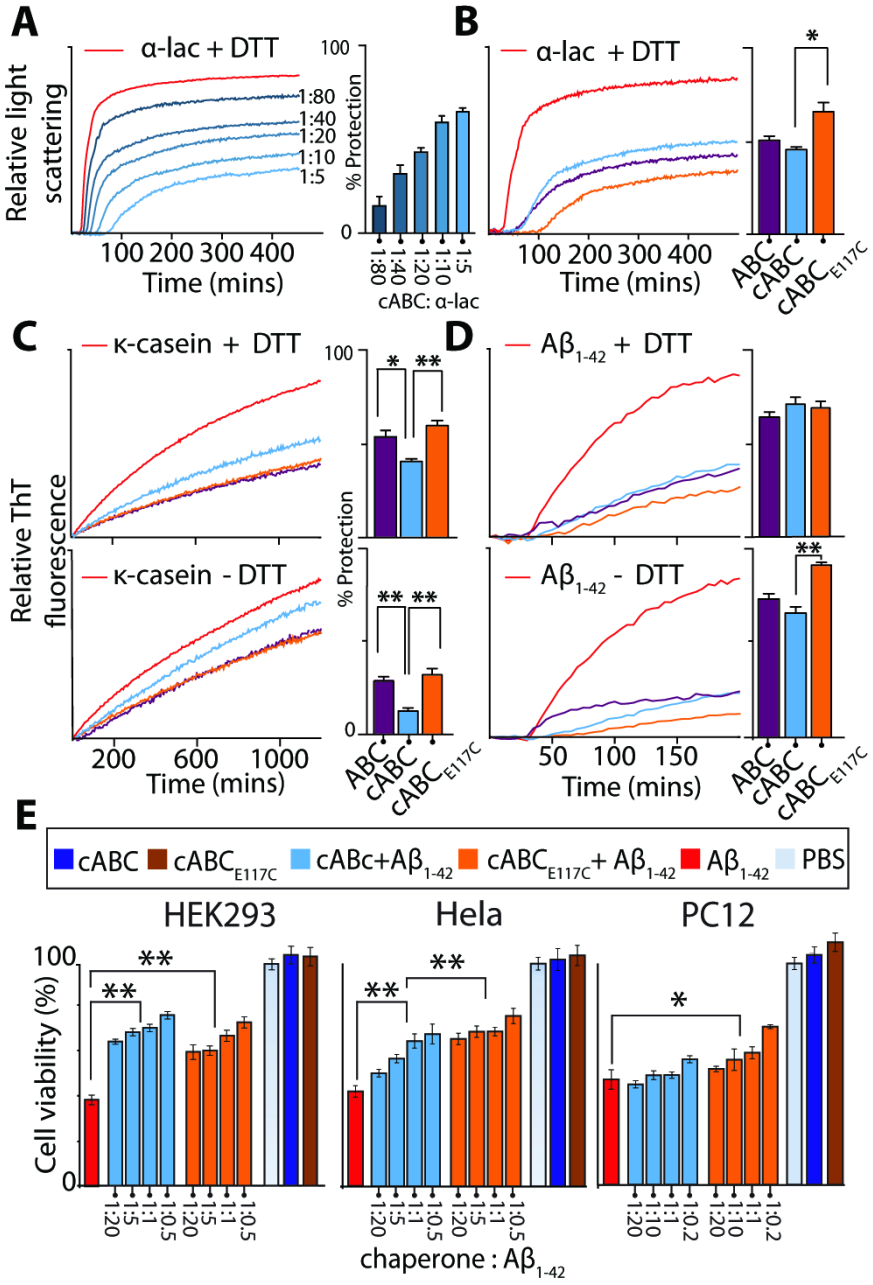

Fig. 5. **Fig. 5:** *In vitro* chaperone activity of ACDs. **(A)** Dose-dependent inhibition of reduction-induced α-lac aggregation by cABC. Molar ratios are indicated as cABC:α-lac. Even at sub-stoichiometric quantities of cABC, significant chaperone activity is observed. **(B)** Comparing different constructs of ABC at a molar ratio of 1:5 (chaperone:α-lac) reveals cABC to be equivalently potent to the full-length protein. $cABC_{E117C}$ is slightly more effective than cABC, likely due to altered surface properties around the introduced cysteine (Fig. S3). **(C)** Assaying κ-casein fibrillation under reducing (upper) and oxidising (lower) conditions in the presence of our ABC constructs at a molar ratio of 1:2 (chaperone: κ-casein) demonstrates that they are capable of slowing aggregation. cABC is less efficient than the full-length protein in both conditions, while $cABC_{E117C}$ is more effective than cABC, mirroring the data in **B**. **(D)** The ABC constructs are also potent inhibitors of $Aβ_{1-42}$ fibrillation at a molar ratio of 1:20 (chaperone:$Aβ_{1-42}$). Under reducing conditions (upper), all three constructs perform equivalently, while under oxidising conditions (lower), $cABC_{E117C}$ is more effective than cABC. This suggests that locking into an AP_{II} dimer improves chaperone action in this assay. In all cases (**A-D**), a representative aggregation assay is shown as well as the percentage protection. Error bars correspond to mean ± standard error of the mean, with n=3. * p<0.05, ** p<0.01. **(E)** Cell viability assays upon addition of $Aβ_{1-42}$ to HEK293, HeLa, and PC12 cells. $Aβ_{1-42}$ on its own (red) causes a decrease in viability to 40 %, while cABC (dark blue), $cABC_{E117C}$ (brown), or buffer (grey) have no effect. $Aβ_{1-42}$ incubated in the presence of increasing amounts of cABC (blue) and $cABC_{E117C}$ (orange) is less toxic than in the absence of chaperone. Molar ratios indicated are chaperone:$Aβ_{1-42}$, with an $Aβ_{1-42}$ concentrationof 0.5 μM in all experiments (except the controls without $Aβ_{1-42}$). In all cases a clear concentration dependence to chaperone protection is observed. Error bars correspond to mean ± standard error of the mean, with n=4. * p<0.05.

intrinsic twist of the monomers (Fig. S1A). Notably, we find that the dimer is in the AP_{III} register, a state previously only observed in the structure of HSP20 (38). A comparison of the registers for ABC reveals the AP_{III} structure to have 685.1 $Å^2$ of buried surface area, compared to 694.1 in AP_{II} (PDB ID: 2WJ7) and 820.7 $Å^2$ in AP_I (3LIG). Together with structures of truncated ABC constructs in the AP_I (41) and AP_{II} states (38-40), this reveals that ABC can populate multiple dimer interface registers that differ in their exposed surface area.

The core domain dimer of HSP27 has cysteines located about a two-fold axis

In order to interrogate the potential role of these different registers we drew inspiration from HSP27, a related human sHSP that has a cysteine residue (C137), located within the β6+7 strand, that can readily be oxidised (44). By employing our co-crystallisation strategy we succeeded in determining the structure for the HSP27 ACD (residues 86-169, cHSP27) in complex with its C-terminal peptide (residues 179-185, ITIPVTF) (Table S1). We find that cHSP27 forms a canonical dimer, in an AP_{II} register, and with the C-terminal peptide bound in an anti-parallel orientation relative to the β8 strand (Fig. 1C). Our structure superimposes well with a previous one in which monomers assembled into a non-canonical hexamer within the crystal lattice (backbone RMSD = 0.45 $Å^2$ comparing monomers, Fig. S1B), and the registration state is consistent with small-angle X-ray scattering data (45). The structures are slightly different around the loop between β5 and β6+7 strands, which contained several point mutations in the previous structure and was disordered. We find this region to be ordered in an extended conformation along the β6+7 sheet of the dimer interface. This can be explained by our construct including additional N-terminal residues, allowing

the formation of a β2 strand consistent with structures obtained for other metazoan ACDs (Fig. S1C).

Differences in the primary sequences of cABC and cHSP27 are distributed over the entire domain, with slightly more disparity observed in flexible loops between successive β-strands (Fig. 2A). While the monomeric fold is nearly identical in the two proteins (Fig. 2B), in cHSP27 the β-sandwich is splayed outward by ≈2.5 Å. This can be attributed to the combined effect of several substitutions (Fig. S1E). The most striking difference, however, is found for residues located next to C137 on the β6+7 strand in HSP27. In cABC there is a charge network of two histidines (H101 and H119) and two glutamates (E99 and E117) that implies pH sensitivity (Fig. 2C) (39, 40). In cHSP27, these histidines are replaced by threonines and E117 by C137, resulting in a disruption of the charge network (Fig. 2C). Moreover, our structure reveals that C137 is located on a central two-fold axis about the dimer interface, and is in a conformation compatible with disulphide bond formation. These differences are consistent with the observation that the ABC dimer interface is pH sensitive (27, 40), and HSP27 activity shows redox dependence (46).

An AP_{II} 'locked' cABC dimer

Motivated by the cHSP27 structure we engineered a cysteine into cABC at position E117, which aligns to C137 in HSP27 (Fig. 2A), and is located about the two-fold axis in the AP_{II} register (Fig. 1C). We crystallized this $cABC_{E117C}$ construct using our co-crystallisation method (Table S1), revealing a fold very similar to cABC and comparable curvature of the dimer interface (Fig. 3A). However, in one of the two dimers comprising the asymmetric unit, this dimer was covalently locked by a disulphide bond between monomers rendering it unable to access registers other than AP_{II} (Fig. 3B). In the locked dimer, the loops between the β5 and β6+7 strands are disordered in the crystal lattice, but are ordered in the other dimer (Chains E and G) (Fig. S2A). There is near-perfect agreement in side-chain positions between cABC and $cABC_{E117C}$ (backbone and side-chain RMSD = 0.33 $Å^2$). The two structures only differ significantly in that the β5 and β6+7 strands are elongated in the AP_{III} register of cABC. The disulphide bond in the $cABC_{E117C}$ structure does not lead to unusual torsion angles in the β-sheet around the bond, nor in the dihedral angles associated with the bond (Fig S2B). While the introduction of strain into anti-parallel β–sheets by disulphide bonds between register-paired cysteines has been proposed as a mechanism of redox regulation (47), our $cABC_{E117C}$ structure hints that redox regulation in HSP27 is achieved via another mechanism.

cABC predominantly populates the AP_{II} register

To assess whether $cABC_{E117C}$ adopts the same monomeric fold as cABC in solution we recorded ^{1}H-^{15}NHSQC NMR spectra for both cABC and $cABC_{E117C}$ under oxidising conditions. In both cases, well-dispersed resonances were observed indicative of a folded structure and consistent with data for similar constructs (43, 48). For most cross-peaks in the cABC spectrum, there is a corresponding cross-peak for oxidized $cABC_{E117C}$ (Fig 3C). Additional cross-peaks are visible in the $cABC_{E117C}$ spectrum that likely result from differences in subunit exchange dynamics between cABC and $cABC_{E117C}$ (48). To assess the magnitude of any changes we determined the change in cross-peak position in both the ^{1}H and ^{15}N dimension (chemical-shift perturbation, CSP) between cABC and $cABC_{E117C}$ based on a previous assignment (48) (Fig, 3D). In most cases the CSPs are <0.16 ppm, which is considerably smaller that those observed in experiments probing the binding of ligands to ABC (43). The two largest CSPs (≈0.7 ppm) are E117 (the site of mutation) and H119, which is hydrogen-bonded to E117 in our cABC structure. Mapping these small CSPs onto the structure of cABC reveals them to cluster around the site of mutation (Fig. 3D), as expected due to the change in chemical environment caused by the substitution of side-chains. The monomeric folds of cABC and $cABC_{E117C}$ in solution are therefore extremely similar, despite $cABC_{E117C}$ being locked into the AP_{II} registration.

To investigate which register cABC populates at equilibrium, we employed ion mobility spectrometry (IM), a technique that reports on the overall size of the molecule in terms of a rotationally averaged collisional cross section (CCS) (49). Theoretical calculations based on the crystal structures of the different forms (Fig. 3B) predict AP_I and AP_{III} to differ from AP_{II} in CCS by -4.5 % and 15.8 %, respectively (Fig. 3E, dashed lines). Comparison of IM data for cABC and $cABC_{E117C}$ under oxidizing conditions however reveals no noticeable differences in CCS distributions (Fig 3E), even though the disulphide-locked $cABC_{E117C}$ is unable to access either AP_I or AP_{III}. This, combined with the similarity of monomeric folds of cABC and $cABC_{E117C}$, indicates that, outside of a crystal lattice, cABC exists predominantly in the AP_{II} register.

The dynamics of $cABC_{E117C}$ under reducing conditions are equivalent to cABC

In order to interrogate the dynamics of cABC we performed nanoelectrospray MS measurements under conditions that preserve non-covalent interactions in vacuum (50). A mass spectrum obtained for cABC features two charge-state distributions, centred on 2000 *m/z* and 2500 *m/z*, which partially overlap and correspond to monomers and dimers, respectively (Fig 4A). At this concentration (8 μM, based on the molar mass of a monomer) a substantial amount of monomer is observed. Increasing the concentration of cABC to 32 μM results in an increasing abundance of dimers (Fig. 4B), consistent with a K_D on the order of a few μM (51). $cABC_{E117C}$ under oxidizing conditions only forms dimers, in line with the disulphide bond formation between monomers observed in the crystal structure (Fig. 4D). Upon the addition of reductant, $cABC_{E117C}$ immediately reverts to a monomer-dimer equilibrium with a K_D comparable to that of cABC (Fig. 4E).

To characterize the kinetics of the monomer-dimer equilibrium in cABC, we performed experiments wherein mass spectra of cABC and a ^{13}C-labelled equivalent were acquired as soon as possible after mixing at 4 °C. Examination of the region of the spectrum corresponding to dimers reveals $^{12}C^{12}C$- and $^{13}C^{13}C$-homodimers, and $^{12}C^{13}C$-heterodimers of cABC. Notably, these three dimeric forms are observed at a 1:1:2 ratio (Fig. 4E), as would be expected statistically upon complete equilibration of this equimolar mixure. As such, complete exchange is reached on a timescale faster than the dead-time of the experiment. This corresponds to a lower limit for the off-rate constant of a monomer from the dimer of 0.1 s^{-1} , approximately five orders of magnitude faster than a monomer dissociating from an oligomer of ABC at the same temperature (27). The equivalent experiment performed for $cABC_{E117C}$ under oxidising conditions shows no subunit exchange, even after prolonged incubation, as anticipated due to the covalent linkage between homodimers. In the presence of reductant, $cABC_{E117C}$ exchanges subunits as rapidly as cABC (Fig. 4D,F). Combined, these results demonstrate that $cABC_{E117C}$ is a redox-sensitive protein that exists as a stable cross-linked dimer under oxidising conditions, and immediately reverts to a monomer-dimer equilibrium with extremely fast subunit exchange dynamics, comparable to those of cABC, upon the addition of reductant.

cABC can prevent amorphous protein aggregation in vitro

The cABC system represent an excellent means to probe the chaperone activity of the core domain itself, and to study the importance of the monomer-dimer equilibrium and its associated subunit-exchange dynamics. In order to investigate this, we assayed the ability of cABC, $cABC_{E117C}$ and full-length ABC to protect three very different targets: α-lactalbumin (α-lac); κ-casein; and the amyloid β-peptide ($Aβ_{1-42}$). These polypeptides differ in their amino-acid sequence, molar mass, mechanism and rate of aggregation, and morphology of the resulting aggregates.

We optimised the chaperone:target molar ratios such that our assays exhibited measurable aggregation of the targets, in order to be sensitive to small differences in chaperone activity.

We first monitored the ability of the different constructs to inhibit the reduction-induced amorphous aggregation of α-lac at 37 °C. In the absence of chaperone, after a lag phase of about 20 minutes, we observed a rapid increase in apparent absorbance due to light scattering (Fig. 5A, red), indicating the aggregation of α-lac (52). Upon addition of cABC, we found a considerable delay to the onset and reduction in the rate of α-lac aggregation (Fig 5A, blue). The extent of protection conferred was strongly dependent on the amount of chaperone, though significant protection ($p<0.01$) was observed even at molar ratios as low as 1:80 (cABC:α-lac). This indicates that cABC affords potent protection against amorphous protein aggregation, at sub-stoichiometric amounts, and in a dose-dependent manner.

In order to quantify the relative efficacy of protection relative to full-length ABC and $cABC_{E117C,}$ we performed a comparative assay at a ratio of 1:5 (chaperone:α-lac). All three chaperones significantly delayed and slowed α-lac aggregation (Fig. 5B). Remarkably, comparison of cABC and full-length ABC reveals no significant difference in their activity. Notably cHSP27, despite being of similar fold to cABC, displayed minimal chaperone activity in this and other assays (Fig. S3). As such it can be regarded as a negative control, and demonstrates the specificity of the chaperone action observed for the constructs of ABC.

In this assay, we find therefore that the ACD in ABC is entirely sufficient for chaperone function (Fig. 5B). Notably, we observe that $cABC_{E117C}$ is more effective at preventing aggregation of α-lac than cABC. It is important to consider that the presence of DTT in this assay means that the disulphide bond in $cABC_{E117C}$ is reduced (Fig. 4F), so this increased activity cannot be ascribed to the exclusive presence of an AP_{II}-locked dimer. Instead we observe that $cABC_{E117C}$ displays increased binding, relative to cABC, of the hydrophobic probe bis-ANS (4,4'-dianilino-1,1'-binaphthyl-5,5'-disulfonic acid), revealing an increased solvent-accessible hydrophobic surface area (Fig. S4). The slight differences in structure between cABC and $cABC_{E117C}$ revealed by our NMR experiments (Fig. 3D) provide one possible rationale for the difference in chaperone activity.

cABC can prevent amyloid fibril formation in vitro

We next tested the ability of cABC to prevent amyloid fibril formation using two model systems: κ-casein and $Aβ_{1-42}$. In these experiments, fibril formation is assayed by monitoring the characteristic red-shift in fluorescence of the dye thioflavin T (ThT) upon binding to amyloid structures. In the absence of chaperone, κ-casein forms fibrils relatively slowly (over a period of >20 hours), without a significant lag phase (Fig. 5C). The timescale of this aggregation is not significantly altered with the presence (upper panel) or absence (lower panel) of the reductant DTT. At a molar ratio of 1:2 (chaperone: κ-casein), ABC slows κ-casein fibril formation under both oxidising and reducing conditions (Fig. 5C). At an equivalent ratio, cABC also retards amyloidogenesis, and only slightly less effectively than the full-length protein. Notably, $cABC_{E117C}$ is more effective at slowing κ-casein aggregation than cABC. This improved activity is observed under both oxidising and reducing conditions, in other words independent of whether the chaperone is locked into AP_{II} dimers. This suggests that the difference in activity in this case is due to the altered surface properties of $cABC_{E117C}$ compared to cABC (Fig. 3D, Fig S4), as observed in our α-lac assay (Fig. 5B).

In order to test our constructs in preventing the aggregation of a target that forms fibrils more rapidly, we assayed their ability to inhibit $Aβ_{1-42}$ amyloidogenesis. In the absence of chaperone, this peptide aggregates over a period of approximately 3 hours, both in the presence and absence of DTT (Fig. 5D). At a molar ratio 1:20 (chaperone:$Aβ_{1-42}$), and in both conditions, we found that all three constructs dramatically slowed aggregation. Notably, no significant difference was observed for cABC relative to the full-length protein (Fig. 5D). Under reducing conditions (upper panel), cABC and $cABC_{E117C}$ have equivalent chaperone ability in this assay. However, under oxidising conditions (lower panel), $cABC_{E117C}$ is more effective at inhibiting $Aβ_{1-42}$ fibril formation than cABC. Therefore, locking cABC into an AP_{II} dimer makes it a more potent chaperone in this assay.

The interaction of cABC with aggregating $Aβ_{1-42}$ reduces toxicity to cells

To test whether the inhibitory effect of cABC on $Aβ_{1-42}$ amyloid formation would result in a decrease in toxicity we performed assays on cultured cells. Specifically we monitored the viability of HEK293, HeLa, and PC12 cells upon the addition of pre-incubated $Aβ_{1-42}$ (Fig. 5E). In all three cell lines, the addition of $Aβ_{1-42}$ resulted in a decrease in viability to about 40%, indicating toxicity of the aggregating peptide. Addition of solutions of $Aβ_{1-42}$ that had been incubated in the presence of chaperone showed a reduction in this toxicity. Notably, not all cell lines responded equivalently, with both cABC and $cABC_{E117C}$ being more effective at rescuing HEK293 and HeLa cells than PC12 cells. While the reasons for this are not known, it is clear that the protective effect was more pronounced with increasing ratios of chaperone:$Aβ_{1-42}$, demonstrating a dose-dependency in all cases. This mirrors data obtained for full-length ABC (19, 20), and reveals that the ACD is sufficient to slow the rate of $Aβ_{1-42}$ aggregation and thereby reduce the toxicity of the aggregating mixture. Interestingly, in these assays that are performed in the absence of reductant, we detect a clear increase in potency for $cABC_{E117C}$ relative to cABC in HeLa cells, and in PC12 only $cABC_{E117C}$ displayed statistically significant potency. This implies that locking cABC into an AP_{II} dimer, which improves its efficacy in slowing the rate of $Aβ_{1-42}$ *in vitro* (Fig. 5D, lower), results in an associated reduction in toxicity of the aggregating mixture.

Discussion

Here we have found that the core domain of ABC is a potent inhibitor of both amorphous and fibrillar aggregation, and amyloid-associated toxicity. Previous reports describing alternatively truncated forms of ABC have shown limited chaperone activity towards other target proteins (41, 53). However, our construct performed comparably to full-length ABC with regards to protecting α-lac and κ-casein from aggregation at sub-stoichiometric levels. Remarkably, our amyloidogenesis and cell toxicity assays of $Aβ_{1-42}$ places cABC among the most potent known inhibitors of $Aβ_{1-42}$ on a molar basis (54). The finding that the ACD can prevent amyloid formation and toxicity is surprising, and raises questions about the role of its flanking and relatively unstructured N- and C- terminal regions, and necessity of the oligomeric form of ABC.

It is important to recognise that our assays report primarily on the ability of the ACD to delay aggregation, and not on the stability of any complexes formed, nor their interactions with the cellular disaggregation, refolding, or degradation machinery (10, 55). Similarly, we are probing only the chaperone function of ABC against selected targets, when it is known that the chaperone has other important roles, including as a major structural component of the eye lens, which may require oligomerisation (56). It is interesting to note that chaperone activity of dimeric sHSPs has been reported from various organisms, including HSP17.7 from *Deinococcus radiodurans* (57), HSP18.5 from *Arabidopsis thaliana* (58), and human HSP20 (59). Although these chaperones do not assemble into oligomers, they still have intact N- and C-termini. Our results clearly demonstrate that the ACD itself can be sufficient for chaperone activity, and is not simply a passive building-block of sHSP oligomers.

We have shown that, against all target proteins tested, $cABC_{E117C}$ locked into an AP_{II} dimer was at least as active as cABC. This demonstrates that dissociation into monomers, subunit exchange dynamics, or accessing other dimer registration states (AP_I or AP_{III}) is not a pre-requisite for the chaperone function of ABC. This observation is consistent with measurements made on an equivalent E117C mutation in full-length ABC, which had activity comparable to the wild-type in preventing rhodanese from aggregating (44). Furthermore, in all our experiments the concentration of chaperone used was close to the K_D of the cABC dimer interface, meaning that a sizeable proportion of the chaperone was monomeric (51). In the case of α-lac and $Aβ_{1-42}$ this did not impair chaperone activity, suggesting that the monomeric ACD is itself chaperone-active. This is consistent with the observation of monomers being the exchanging unit in ABC (27). Taken together with the observation that full-length ABC is active, including when cross-linked to prevent its dissociation (36), a picture emerges wherein the ACD is chaperone-active, and its binding surfaces accessible, irrespective of its quaternary state.

Hydrophobic interactions are often hypothesized as the likely mode of chaperone-target interactions (5, 6). Interestingly, cABC has few exposed hydrophobic patches, and has fewer than the structurally similar, yet inactive cHSP27 (Fig. S4). Although we did measure an increase in exposed hydrophobic surface area in $cABC_{E117C}$ relative to cABC (Fig. S4), we did not detect major structural distortions in the monomeric fold due to the mutation in either our NMR or X-ray crystallography experiments. It is possible therefore, that the increased chaperone activity of $cABC_{E117C}$ may be due to residue 117 being proximal to the binding site of cABC, and mutation to cysteine resulting in favourable changes to the protein surface. Alternatively, we have established previously that the dimer interface and the β4-β8 groove that accommodates the C-terminal peptide are allosterically coupled: strengthening of one results in the weakening of the other (27, 51). As such, it may be that stabilising the dimer interface through the covalent linkage may increase the accessibility of the groove as a potential site for target binding.

While cABC is an effective chaperone against the aggregation of all the targets assayed here, there nonetheless remain differences in effectiveness of protection compared to full-length ABC. In the case of α-lac, the core is entirely sufficient for chaperone function, whereas with κ-casein it is somewhat less active than full-length ABC. The effect of the E117C mutation resulted in an increase in potency against α-lac and κ-casein regardless of its redox state, which could be rationalised by slight differences in surface hydrophobicity (Fig. S4). Interestingly, $cABC_{E117}$ was also more potent against $Aβ_{1-42}$ aggregation than cABC, but only when the disulphide bond locked $cABC_{E117}$ into a dimeric form. Combined, this suggests there are subtle differences in the way the ACD interacts with different targets, perhaps through separate parts of its molecular surface. This is consistent with observations of different modes of action for amorphous and amyloidogenic aggregation (60, 61), and chaperone activity for peptides from different regions of ABC (31, 32).

It is important to note that sequence differences between cABC and the chaperone inactive cHSP27 are distributed all over the surface, and do not cluster around either the dimer interface or the β4-β8 groove (Fig. 2). The small number of differences in primary amino acid sequence therefore does not point to any particular patch of the domain that renders cABC active and cHSP27 inactive. Irrespective of the exact location of the binding site on cABC, the similarity of the cABC and cHSP27 structures suggests that specific residues mediate the interaction between cABC and the targets assayed here. Importantly, the system and approaches we have developed will enable us to probe structurally this important function of sHSP. Understanding how such a small folded protein inhibits amyloid toxicity will potentially be of great use in the search for effective biotherapeutic strategies for diseases associated with amyloid fibril formation.

Materials and methods

ABC, cABC and cHSP27 protein expression and purification

Human ABC, cABC (residues 68-153) and cHSP27 (residues 84-176) were cloned, expressed and purified as described previously (41, 51), with the exception that in the His-tag buffers phosphate was replaced by TRIS. Truncated proteins were expressed with N-terminal TEV protease cleavable His-tags and purified by using nickel-affinity chromatography. The N-terminal His-tag was removed with TEV protease and the protein buffer exchanged using either a Superdex 75 gel filtration column (GE Healthcare) or two 5 mL HiTrap desalting columns (GE Healthcare) connected in series. For subunit exchange experiments, cABC was expressed in M9 minimal media containing ^{13}C-labelled D-glucose as the only carbon source and purified as described above. For NMR experiments, cABC and $cABC_{E117C}$ were expressed in M9 minimal media containing ^{15}N ammonium chloride as the only nitrogen source.

ABC and HSP27 C-terminal peptide expression and purification

The C-terminal peptides (ABC residues 156-164, ERTIPITRE; HSP27 residues 179-185, ITIPVTF) were either purchased (Biomatik or Genscript), or expressed recombinantly and purified as described previously (62). Briefly, an expression construct containing an N-terminal His-tagged maltose binding protein followed by a TEV protease cleavage site in pET15b (Novagen) was amplified by PCR using a T7 forward primer and reverse primer with a 5' overhang containing the DNA sequence for the C-terminal peptide followed by a stop codon and XhoI restriction site. The subsequent PCR product was digested with NdeI and XhoI (New England Biolabs) followed by ligation using a Quick Ligation kit (New England Biolabs) into pET28b. The fusion construct was expressed and purified using nickel-affinity chromatography followed by TEV protease cleavage, leaving an additional N-terminal glycine, and purification using reverse-phase high performance liquid chromatography. Peptide fractions were verified by means of MS, and stored in desiccant jars at -20 □°C.

Crystallization of cABC and cHSP27 in complex with their C-terminal peptides

Crystals were grown in hanging-drop plates (VDX, Hampton Research) at room temperature. A final mixture containing 8-10 mg/mL monomer supplemented with 2-3 fold molar excess of the appropriate C-terminal peptide (10 mM stock, in water) was prepared in X-tal buffer (100 mM sodium chloride, 20 mM TRIS, pH 8.0). Crystals of cABC with recombinant C-terminal peptide grew in 0.1 M SPG (succinic acid, dihydrogen phosphate, glycine) buffer pH 6.0 and 25 % PEG 1500. Crystals of $cABC_{E117C}$ with synthetic C-terminal peptide grew in 0.085 M MES pH 6.5, 0.17 M ammonium sulphate, 25.5 % PEG 5000 MME, and 15 % glycerol. A final mixture containing 9 mg/mL cHSP27 supplemented with 2-fold molar excess of the synthetic C-terminal peptide (10mM stock, in water) prepared in Xtal buffer supplemented with 1mM DTT was crystallized in Crystal Screen (Hampton Research) condition #6 (0.2 M magnesium chloride, 0.1M TRIS pH 8.5, and 30 % PEG 4,000). With the exception of $cABC_{E117C}$, crystals were cryo-protected in mother-liquid solution containing 20 % glycerol. All crystals were flash-frozen in liquid nitrogen.

Structure determination and analysis

X-ray diffraction data were processed using XDS (63), and structures determined by molecular replacement using Phaser (64), followed by automated model building using Phenix (65). Models were built using Coot (66) and refined with REFMAC (67), Phenix (65), and Buster (68). Structures of cABC, $cABC_{E117C}$, and cHSP27 have been deposited in the PDB with accession codes 4M5S, 4M5T, 4MJH respectively.

Buried surface areas in the dimer interface were calculated using the PISA server (69). 3L1G and 2WJ7 were used for calculations for AP_I and AP_{II}. Sequence alignments were generated using the ClustalW2 server (70). Amino acids were coloured according to their score in the Gonnet Pam250 matrix generated by the ClustalW2 server (<0:red; =<0.5:orange, >0.5:yellow), and fully conserved residues were not coloured (Fig. 2A). Surface hydrophobicity was calculated and rendered using the UCSF Chimera (71).

Mass spectrometry

MS measurements were carried out on a IM QToF (Synapt G1, Waters) modified to incorporate a linear drift tube (72). Nanoelectrospray mass spectra were acquired under conditions optimised for the preservation of noncovalent interactions essentially as described previously (51) and with the following instrument parameters: sample cone 10 V, extraction cone 5 V, trap 10 V, trap gas (argon): 2.6 ml/min, drift-cell pressure (helium) 2.14 Torr. Unless stated otherwise, samples were analysed at monomeric concentrations of 10-20 μM in 200 mM ammonium acetate pH 6.9. DTT, to a final concentration of 5 mM, was added where stated. For subunit exchange experiments, ^{13}C-labelled and unlabelled protein was mixed at equimolar ratios at 4 °C and analysed by MS as soon as possible after mixing (<1 min). CCSs were measured by mixing oxidized $cABC_{E11C}$ and ^{13}C-labelled cABC, and then recording spectra at nine drift voltages in the range 50-200 V. At each drift voltage, arrival times were fitted to normal distributions, and the transport time (T_0) of ions from the exit of the drift-tube region to the time-of-flight analyzer obtained (72). CCS distributions were obtained from the

arrival time (T_a) distributions of the 7+ charge state at each drift voltage V_D using $CCS = 4.482 \times 10^{-3}(T_a - T_c)V_D zTP^{-1}$ where z is the charge of the ion, T is the temperature in K, P the pressure in Torr, and the constant amalgamates the length of the drift tube with the necessary components of the Mason-Schamp equation (49, 72). The data from all drift voltages were combined and fitted globally to a normal distribution. Theoretical CCSs of AP_I-AP_{III} were calculated from the cABC crystal structure using CCSCalc (Waters) with a gas radius of 1 Å and tolerance of 0.1%, and normalized to the experimentally determined CCS value of AP_{II} for comparison.

NMR spectroscopy

NMR experiments were performed on a 600 MHz spectrometer (Varian) equipped with a 5 mm z-axis gradient triple-resonance probe. ^{15}N-labelled cABC and $cABC_{E117C}$ were prepared in 25 mM sodium phosphate, 2 mM EDTA, 2 mM sodium azide, pH 7.5 and concentrated to 500 µM using amicon concentrators (Millipore, UK). 2D ^{15}N-^{1}H HSQC correlation spectra were recorded with 8 scans per transient with acquisition times (t_1, t_1) of (65.8, 135.1) ms, over (608, 100) complex points and a 1 s relaxation delay, for a total acquisition time of 26 min. All spectra were analysed using NMRPipe (73) and Sparky (T. D. Goddard and D. G. Kneller, University of California, San Francisco). Peaks were ascribed to particular residues based on the previous assignment of a similar construct (74). To measure chemical shift perturbations (CSPs) in both dimensions, the chemical shift difference in the nitrogen dimension was divided by 5 to account for the distribution of shifts recorded in the BMRB. In the few cases where several peaks could not be clearly assigned in the $cABC_{E117C}$ spectrum, the furthest peak was used for CSP calculations in order not to under-estimate the CSP. If the closest peak was used instead, the pattern of CSPs was very similar, although the CSPs were slightly smaller (Fig. S2C, D).

In vitro protein aggregation assays

The aggregation and precipitation of the target proteins, reported via either ThT fluorescence or light-scattering assays, was monitored by using sealed 96-microwell plates and Fluostar Optima plate reader (BMG Labtechnologies). The amorphous aggregation of α-lac (Sigma-Aldrich, 100 µM), incubated at 37 °C in 50 mM phosphate buffer containing 100 mM NaCl and 5 mM EDTA, pH 7.0, was initiated by the addition of DTT (20 mM). Chaperones were added at the molar ratios stated. Aggregation was monitored by measuring the change in apparent absorbance due to light scattering at 340 nm, which was negligible in the absence of α-lac. The formation of amyloid fibrils by target proteins was monitored using an *in situ* ThT-binding assay (75). κ-casein (Sigma-Aldrich, 50 µM) was incubated at 37 °C in 50 mM phosphate buffer (pH 7.4), and $A\beta_{1\text{-}42}$ (Anaspec, 10 µM) at 37 °C in PBS (pH 7.4). Chaperones and DTT (20 mM) were added where stated at a molar ratio of 1:2 (chaperone:κ-casein) or 1:20 (chaperone:$A\beta_{1\text{-}42}$). Samples were incubated with 10 µM ThT and the fluorescence levels measured with a 440/490 nm excitation/emission filter set. The change in ThT fluorescence in the absence of either κ-casein or $A\beta_{1\text{-}42}$ was negligible for each assay. In all cases, the relative ability of each chaperone to prevent aggregation was evaluated by comparing the apparent absorbance/ThT fluorescence at the end of each assay, as previously described (76). Data are reported as mean ± SEM (n = 3) and were analysed by one-way ANOVA and Tukey's post-hoc test. To assay exposed hydrophobicity, samples were prepared at 2.5 µM in PBS and bis-ANS was added to a final concentration of 10 µM. Fluorescence spectra were recorded as previously described (60).

Cell viability assays

Cell viability was measured by using a CellTiter 96 aqueous non-radioactive cell proliferation assay kit (Promega #G4100). PC-12 (ATCC cat. # CRL-1721), HeLa and HEK293 cell lines were used to assess the inhibition of our ABC constructs on $A\beta_{1\text{-}42}$ toxicity. HeLa and HEK293 cells were cultured in DMEM medium with 10% fetal bovine serum. PC12 cells were cultured in ATCC-formulated RPMI 1640 medium (ATCC) with 10% heat-inactivated horse serum and 5% fetal bovine serum. All cells were maintained at 5% CO_2 at 37 °C. For cell viability measurements, HeLa, HEK293 and PC-12 cells were plated out in 96-well plates (Costar) at 10000 cells/well, and cultured for 20 h at 37 °C in 5% CO_2 before adding different incubation mixtures. These were prepared to a final concentration of 5 µM $A\beta_{1\text{-}42}$ monomer in PBS (pH 7.4), in the presence or absence of chaperone as indicated, and incubated at 37 °C for 18 h. 10 µL of incubated sample was added to each well containing 90 µL cell suspension. After 24 h incubation, 15 µL "dye" solution was added to each well, and the cells incubated for a further 4 h before the addition of 100 µL "solution/stop mix" to each well. After incubation at room temperature for 12 h, the absorbance of each well was measured at 570 nm, with the background absorbance recorded at 700 nm. The final data were normalized by using the buffer-treated cell as 100% viability and 0.2% SDS-treated cell as 0% viability. Data are reported as mean ± SEM (n = 4) and the titration series were analysed globally using an unpaired Student's T-test. Specifically, the plateau of viability at high ratios of chaperone: $A\beta_{1\text{-}42}$ was determined by fitting the data to an exponential rise to maximum (77), and compared to the absence of chaperone altogether.

\body

Acknowledgements.

GKAH is supported by an EPSRC studentship held at the Systems Biology Doctoral Training Centre. HE is supported by an Australian Research Council Future Fellowship (FT110100586) and Australian Department of Health and Ageing seed grant. D Cox is supported by an Australian post-graduate award. MPC was supported for a summer internship by a National Scholarship from the University of Alabama at Birmingham. AJB holds a David Phillip's Fellowship of the Biotechnology and Biological Sciences Research Council. CVR is a Royal Society Professor. DE thanks NSF-MCB-095811 and NIH AG029430 for support. JLPB is a Royal Society University Research Fellow, and AL a Nicholas Kurti Junior Research Fellow of Brasenose College, Oxford.

1. Baldwin A, *et al.* (2011) Metastability of Native Proteins and the Phenomenon of Amyloid Formation. *J Am Chem Soc* 133(36):14160-14163.
2. Olzscha H, *et al.* (2011) Amyloid-like aggregates sequester numerous metastable proteins with essential cellular functions. *Cell* 144(1):67-78.
3. Powers ET & Balch WE (2013) Diversity in the origins of proteostasis networks--a driver for protein function in evolution. *Nat Rev Mol Cell Biol* 14(4):237-248.
4. Balch WE, Morimoto RI, Dillin A, & Kelly JW (2008) Adapting proteostasis for disease intervention. *Science* 319(5865):916-919.
5. Hartl FU, Bracher A, & Hayer-Hartl M (2011) Molecular chaperones in protein folding and proteostasis. *Nature* 475(7356):324-332.
6. Richter K, Haslbeck M, & Buchner J (2010) The heat shock response: life on the verge of death. *Mol Cell* 40(2):253-266.
7. Basha E, O'Neill H, & Vierling E (2011) Small heat shock proteins and alpha-crystallins: dynamic proteins with flexible functions. *Trends Biochem Sci* 37(3):106-17.
8. Hilton GR, Lioe H, Stengel F, Baldwin AJ, & Benesch JL (2013) Small heat-shock proteins: paramedics of the cell. *Top Curr Chem* 328:69-98.
9. McHaourab HS, Godar JA, & Stewart PL (2009) Structure and mechanism of protein stability sensors: chaperone activity of small heat shock proteins. *Biochemistry* 48(18):3828-3837.
10. Carra S, *et al.* (2013) Different anti-aggregation and pro-degradative functions of the members of the mammalian sHSP family in neurological disorders. *Phil T Roy Soc B* 368(1617):20110409.
11. Garrido C, Paul C, Seigneuric R, & Kampinga HH (2012) The small heat shock proteins family: the long forgotten chaperones. *Int J Biochem Cel* 44(10):1588-1592.
12. Horwitz J (1992) Alpha-crystallin can function as a molecular chaperone. *Proc Natl Acad Sci USA* 89(21):10449-10453.
13. Boncoraglio A, Minoia M, & Carra S (2012) The family of mammalian small heat shock proteins (HSPBs): implications in protein deposit diseases and motor neuropathies. *Int J Biochem Cel* 44(10):1657-1669.
14. Ecroyd H & Carver JA (2009) Crystallin proteins and amyloid fibrils. *Cell. Mol. Life Sci.* 66(1):62-81.
15. Kampinga HH & Garrido C (2012) HSPBs: small proteins with big implications in human disease. *Int J Biochem Cell* 44(10):1706-1710.
16. Chiti F & Dobson CM (2006) Protein misfolding, functional amyloid, and human disease. *Annu Rev Biochem* 75:333-366.
17. Eisenberg D & Jucker M (2012) The amyloid state of proteins in human diseases. *Cell* 148(6):1188-1203.
18. Haass C & Selkoe DJ (2007) Soluble protein oligomers in neurodegeneration: lessons from the Alzheimer's amyloid beta-peptide. *Nat Rev Mol Cell Biol* 8(2):101-112.
19. Wilhelmus M, *et al.* (2006) Small heat shock proteins inhibit amyloid-beta protein aggregation and cerebrovascular amyloid-beta protein toxicity. *Brain Res* 1089(1):67-78.
20. Mannini B, *et al.* (2012) Molecular mechanisms used by chaperones to reduce the toxicity of aberrant protein oligomers. *Proc Natl Acad Sci USA* 109(31):12479-12484.
21. Knowles TP, *et al.* (2007) Kinetics and thermodynamics of amyloid formation from direct measurements of fluctuations in fibril mass. *Proc Natl Acad Sci USA* 104(24):10016-10021.
22. Raman B, *et al.* (2005) AlphaB-crystallin, a small heat-shock protein, prevents the amyloid fibril growth of an amyloid beta-peptide and beta2-microglobulin. *Biochem J* 392(Pt 3):573-581.
23. Rekas A, *et al.* (2004) Interaction of the molecular chaperone alphaB-crystallin with alpha-synuclein: effects on amyloid fibril formation and chaperone activity. *J Mol Biol* 340(5):1167-1183.
24. Shammas SL, *et al.* (2011) Binding of the molecular chaperone alphaB-crystallin to Abeta amyloid fibrils inhibits fibril elongation. *Biophys J* 101(7):1681-1689.
25. Waudby C, *et al.* (2010) The interaction of alphaB-crystallin with mature alpha-synuclein amyloid fibrils inhibits their elongation. *Biophys J* 98(5):843-851.
26. Binger KJ, *et al.* (2013) Avoiding the oligomeric state: alphaB-crystallin inhibits fragmentation and induces dissociation of apolipoprotein C-II amyloid fibrils. *FASEB J* 27(3):1214-1222.
27. Baldwin AJ, Lioe H, Robinson CV, Kay LE, & Benesch JLP (2011) αB-crystallin polydispersity is a consequence of unbiased quaternary dynamics. *J Mol Biol* 413(2):297-309.
28. Aquilina JA, Shrestha S, Morris AM, & Ecroyd H (2013) Structural and functional aspects of hetero-oligomers formed by the small heat shock proteins alphaB-crystallin and HSP27. *J Biol Chem* 288(19):13602-13609.
29. Delbecq SP & Klevit RE (2013) One size does not fit all: the oligomeric states of alphaB crystallin. *FEBS Lett* 587(8):1073-1080.
30. Aquilina JA & Watt SJ (2007) The N-terminal domain of alpha B-crystallin is protected from proteolysis by bound substrate. *Biochem Biophys Res Commun* 353(4):1115-1120.
31. Bhattacharyya J, Padmanabha Udupa EG, Wang J, & Sharma KK (2006) Mini-alphaB-crystallin: a functional element of alphaB-crystallin with chaperone-like activity. *Biochemistry* 45(9):3069-3076.
32. Ghosh JG, Estrada MR, & Clark JI (2005) Interactive domains for chaperone activity in the small heat shock protein, human crystallin. *Biochemistry* 44(45):14854-14869.
33. Narayanan S, Kamps B, Boelens WC, & Reif B (2006) alphaB-crystallin competes with

Alzheimer's disease beta-amyloid peptide for peptide-peptide interactions and induces oxidation of Abeta-Met35. *FEBS Lett* 580(25):5941-5946.
34. Sharma KK, Kaur H, & Kester K (1997) Functional elements in molecular chaperone alpha-crystallin: identification of binding sites in alpha B-crystallin. *Biochem Biophys Res Commun* 239(1):217-222.
35. Bova MP, Ding LL, Horwitz J, & Fung BKK (1997) Subunit exchange of alpha A-crystallin. *J Biol Chem* 272(47):29511-29517.
36. Augusteyn RC (2004) Dissociation is not required for alpha-crystallin's chaperone function. *Exp Eye Res* 79(6):781-784.
37. Aquilina JA, *et al.* (2005) Subunit exchange of polydisperse proteins: mass spectrometry reveals consequences of alphaA-crystallin truncation. *J Biol Chem* 280(15):14485-14491.
38. Bagneris C, *et al.* (2009) Crystal structures of alpha-crystallin domain dimers of alphaB-crystallin and Hsp20. *J Mol Biol* 392(5):1242-1252.
39. Clark AR, Naylor CE, Bagneris C, Keep NH, & Slingsby C (2011) Crystal structure of R120G disease mutant of human alphaB-crystallin domain dimer shows closure of a groove. *J Mol Biol* 408(1):118-134.
40. Jehle S, *et al.* (2010) Solid-state NMR and SAXS studies provide a structural basis for the activation of alphaB-crystallin oligomers. *Nat Struct Mol Biol* 17(9):1037-1042.
41. Laganowsky A, *et al.* (2010) Crystal structures of truncated alphaA and alphaB crystallins reveal structural mechanisms of polydispersity important for eye lens function. *Protein Sci* 19(5):1031-1043.
42. Laganowsky A & Eisenberg D (2010) Non-3D domain swapped crystal structure of truncated zebrafish alphaA crystallin. *Protein Sci* 19(10):1978-1984.
43. Delbecq SP, Jehle S, & Klevit R (2012) Binding determinants of the small heat shock protein, alphaB-crystallin: recognition of the 'IxI' motif. *EMBO J* 31(24):4587-4594.
44. Mymrikov EV, Bukach OV, Seit-Nebi AS, & Gusev NB (2010) The pivotal role of the beta 7 strand in the intersubunit contacts of different human small heat shock proteins. *Cell Stress Chaperon* 15(4):365-377.
45. Baranova EV, *et al.* (2011) Three-Dimensional Structure of alpha-Crystallin Domain Dimers of Human Small Heat Shock Proteins HSPB1 and HSPB6. *J Mol Biol* 411(1):110-122.
46. Arrigo AP (2001) Hsp27: novel regulator of intracellular redox state. *IUBMB Life* 52(6):303-307.
47. Indu S, Kochat V, Thakurela S, Ramakrishnan C, & Varadarajan R (2011) Conformational analysis and design of cross-strand disulfides in antiparallel beta-sheets. *Proteins* 79(1):244-260.
48. Jehle S, *et al.* (2009) [alpha]B-Crystallin: A Hybrid Solid-State/Solution-State NMR Investigation Reveals Structural Aspects of the Heterogeneous Oligomer. *J Mol Biol* 385(5):1481-1497.
49. Ruotolo BT, Benesch JL, Sandercock AM, Hyung SJ, & Robinson CV (2008) Ion mobility-mass spectrometry analysis of large protein complexes. *Nat Protoc* 3(7):1139-1152.
50. Benesch JLP & Ruotolo BT (2011) Mass Spectrometry: an Approach Come-of-Age for Structural and Dynamical Biology. *Curr Opin Struct Biol* 21(5):641-649.
51. Hilton GR, *et al.* (2013) C-terminal interactions mediate the quaternary dynamics of alphaB-crystallin. *Phil T Roy Soc B* 368(1617):20110405.
52. Carver J, *et al.* (2002) The Interaction of the Molecular Chaperone Œ±-Crystallin with Unfolding α-Lactalbumin: A Structural and Kinetic Spectroscopic Study. *J Mol Biol* 318(3):815-827.
53. Feil IK, Malfois M, Hendle J, van der Zandt H, & Svergun DI (2001) A novel quaternary structure of the dimeric alpha-crystallin domain with chaperone-like activity. *J Biol Chem* 276(15):12024-12029.
54. Hard T & Lendel C (2012) Inhibition of amyloid formation. *J Mol Biol* 421(4-5):441-465.
55. Liberek K, Lewandowska A, & Zietkiewicz S (2008) Chaperones in control of protein disaggregation. *EMBO J* 27(2):328-335.
56. Piatigorsky J & Wistow G (1991) The recruitment of crystallins: new functions precede gene duplication. *Science* 252(5009):1078-1079.
57. Bepperling A, *et al.* (2012) Alternative bacterial two-component small heat shock protein systems. *Proc Natl Acad Sci USA* 109(50):20407-20412.
58. Basha E, *et al.* (2013) An unusual dimeric small heat shock protein provides insight into the mechanism of this class of chaperones. *J Mol Biol* 425(10):1683-1696.
59. Bukach OV, Seit-Nebi AS, Marston SB, & Gusev NB (2004) Some properties of human small heat shock protein Hsp20 (HspB6). *FEBS J* 271(2):291-302.
60. Kulig M & Ecroyd H (2012) The small heat-shock protein alphaB-crystallin uses different mechanisms of chaperone action to prevent the amorphous versus fibrillar aggregation of alpha-lactalbumin. *Biochem J* 448(3):343-352.
61. Ecroyd H, *et al.* (2008) Dissociation from the oligomeric state is the rate-limiting step in fibril formation by kappa-casein. *Biol Chem* 283(14):9012-9022.
62. Laganowsky A, *et al.* (2012) Atomic view of a toxic amyloid small oligomer. *Science* 335(6073):1228-1231.
63. Kabsch W (1993) Automatic processing of rotation diffraction data from crystals of initially unknown symmetry and cell constants. *J Appl Crystallogr* 26(6):795-800.
64. McCoy AJ, *et al.* (2007) Phaser crystallographic software. *J Appl Crystallogr* 40(Pt 4):658-674.
65. Adams PD, *et al.* (2002) PHENIX: building new software for automated crystallographic structure determination. *Acta Crystallogr D Biol Crystallogr* 58(Pt 11):1948-1954.
66. Emsley P, Lohkamp B, Scott WG, & Cowtan K (2010) Features and development of Coot. *Acta Crystallogr D Biol Crystallogr* 66(Pt 4):486-501.
67. Murshudov GN, Vagin AA, & Dodson EJ (1997) Refinement of macromolecular structures by the maximum-likelihood method. *Acta Crystallogr D Biol Crystallogr* 53(Pt 3):240-255.
68. Smart OS, *et al.* (2012) Exploiting structure similarity in refinement: automated NCS and target-structure restraints in BUSTER. *Acta Crystallogr D Biol Crystallogr* 68(Pt 4):368-380.
69. Krissinel E & Henrick K (2007) Inference of macromolecular assemblies from crystalline state. *J Mol Biol* 372(3):774-797.
70. Larkin MA, *et al.* (2007) Clustal W and Clustal X version 2.0. *Bioinformatics* 23(21):2947-2948.
71. Pettersen EF, *et al.* (2004) UCSF Chimera--a visualization system for exploratory research and analysis. *J Comput Chem* 25(13):1605-1612.
72. Bush MF, *et al.* (2010) Collision cross sections of proteins and their complexes: a calibration framework and database for gas-phase structural biology. *Anal Chem* 82(22):9557-9565.
73. Delaglio F, *et al.* (1995) NMRPipe: a multidimensional spectral processing system based on UNIX pipes. *J Biomol NMR* 6(3):277-293.
74. Jehle S, *et al.* (2011) N-terminal domain of alphaB-crystallin provides a conformational switch for multimerization and structural heterogeneity. *Proc Natl Acad Sci USA* 108(16):6409-6414.
75. Ecroyd H, *et al.* (2008) Dissociation from the oligomeric state is the rate-limiting step in fibril formation by kappa-casein. *J Biol Chem* 283(14):9012-9022.
76. Ecroyd H & Carver J (2008) The effect of small molecules in modulating the chaperone activity of alphaB-crystallin against ordered and disordered protein aggregation. *FEBS J* 275(5):935-947.
77. Slob W (2002) Dose-Response Modeling of Continuous Endpoints. *Toxicol Sci* 66(2):298-312.